JTE
HCMUTE
ISSN: 2615-9740

JOURNAL OF TECHNICAL EDUCATION SCIENCE
Ho Chi Minh City University of Technology and Education
Website: https://jte.edu.vn
Email: jte@hcmute.edu.vn

Design of the Adaptive Neuro-Fuzzy Inference System (ANFIS) and a Genetic Algorithm Controller for Solar Photovoltaic Systems Using the Boost Converter

Thanh Ha Vo
Faculty of Electrical and Electronics Engineering, University of Transport and Commucations, Vietnam

* Corresponding author. *Email: vothanhha.ktd@utc.edu.vn*

ARTICLE INFO

Received: 02/08/2023
Revised: 08/08/2023
Accepted: 09/08/2023
Published: 28/08/2023

KEYWORDS

GA;
ANFIS;
PI;
MPPT;
PV.

ABSTRACT

The Adaptive Neuro-Fuzzy Inference System (ANFIS) and an integrated offline Genetic Algorithm (GA) are proposed in this research. The ANFIS and GA technologies are employed to find the optimum point for maximum capacity in any environmental condition. Furthermore, a genetic algorithm is used to optimize data, and optimized values are used to train ANFIS. The power from the PV source is routed via the standard PI-controlled boost converter, and its working point always follows the MPPT point. When the ambient temperature and illuminance vary, the power may rapidly achieve a new maximum value thanks to the GA-ANFIS-MPPT P&O algorithm, which permits adaptive adjustment of the perturbation step. The new algorithm also reduces oscillation over the whole working point of the MPPT and enhances the boost converter's output voltage quality. The adaptive GA-ANFIS-MPPT P&O algorithm's benefit is validated by simulation on MATLAB has a module string, one parallel string, and a 250W PV panel. According to simulation results, the proposed GA-ANFIS-based MPPT can consistently and efficiently monitor the maximum power point of PV modules across various weather conditions.

Doi: https://doi.org/10.54644/jte.78A.2023.1439

1. Introduction

Renewable energy plays a vital role in electricity production. Renewable energy sources, as different as solar and wind energy, have been mined to generate electrical power. In which, energy solar energy is now a potential choice because it is an available and clean energy source [1]. Solar is directly converted to electricity by the solar photovoltaic (PV) battery module. PV modules with PowerPoint maximum (MPP - Maximum Power Point) corresponding to ambient conditions such as solar radiation, the temperature of tissues PV module, cell area, and load. Let the PV module generate peak power, extreme power tracking methods. Modern technology (MPPT) has always been interested in applied research in stand-alone and grid-connected PV systems [2]. However, solar PV depends on radiation and temperature to generate electricity. These factors vary according to atmospheric conditions, weather, climate, and seasons. Other states, such as partial shade due to cloud cover, nearby trees, buildings, and dust, also adversely affect PV-based power generation [3]. Therefore, the problem of optimizing the maximum capacity of PV panels is essential [4]. The leading power optimization and top power point tracking methods are commonly used, such as the shuffle and observe (MPPT P&O) method and the incremental conductance method (MPPT IC). Many repeated oscillations around the maximum value of the monitored power characterize these two methods. As a result, they are not accurate when predicting maximum PV panel capacity under adverse weather conditions. However, they are easy to design and implement [5]-[8]. Control solutions to reduce or eliminate the disadvantages of MPPT P&O and MPPT IC methods effectively use fuzzy logic-based controllers and neurons. However, the fuzzy-based MPPT controller relies heavily on the precise design of fuzzy rules and membership functions [9]. The ANN-based MPPT controller has disadvantages, such as needing a large amount of training data to ensure accuracy, longer training time, and higher complexity of ANN architecture design [10]-[12]. From the above results, the paper realizes that it is necessary always to maintain the optimal operating point of the solar power system capacity and propose advanced solutions to overcome the shortcomings of the

JTE
HCMUTE
ISSN: 2615-9740

JOURNAL OF TECHNICAL EDUCATION SCIENCE
Ho Chi Minh City University of Technology and Education
Website: https://jte.edu.vn
Email: jte@hcmute.edu.vn

above control. The controller combines a genetic algorithm with a fuzzy - neuron. The best approach for mapping the input-output of nonlinear functions is ANN. However, identifying member functions and fuzzy logic control rules - FLC depends on prior system information. A sophisticated AI approach called ANFIS may be produced by combining neural networks with fuzzy logic [13]. The current research suggests a hybrid model for very short-term forecasting. It is based on combining a Genetic Algorithm (GA) and an Adaptive Neuro-Fuzzy Inference System (ANFIS) to monitor PV power under diverse conditions caused by climate change. In ANFIS, GA optimizes training data. This work uses 360-degree temperature and irradiance data as input data for the genetic algorithm GA, and Vmpp corresponds to the distribution of MPP from a solar system—the principles To train ANFIS, the best value is chosen [14]-[17].

This paper is structured as follows: Section 2 describes the construction of the solar module. Section 3 is expressed for partially discussing the GA and ANFIS algorithm. Section 4 will be presented a boost converter. Section 4 is the simulation findings. Section 5 finally describes the conclusion.

2. Model of Solar Photovoltaic

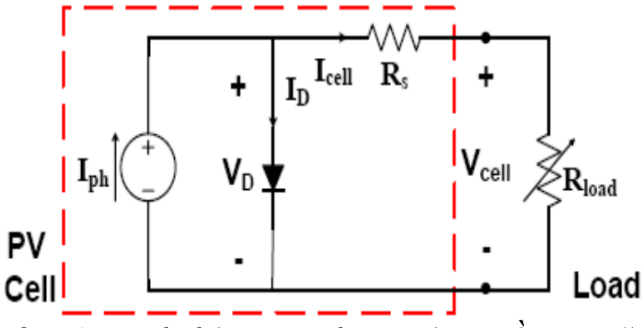

Figure 1. *Circuit diagram of solar cell source PV*

The nonlinear equation of V-I characteristics of PV solar energy source including Ns cells connected in series and N_p cells connected in parallel has the following form:

$$V_g = -I_g R_s \left(\frac{N_s}{N_p}\right) + \left(\frac{N_s}{A}\right).ln\left\{1 + N_s I_{ph} - \frac{N_s}{N_p I_0}\right\} \quad (1)$$

where: A = q/AKT; q – electric charge; A – completion factor; K – constant Boltzmann; T – absolute temperature.

The equivalent circuit of the PV solar cell is shown in Figure 1.

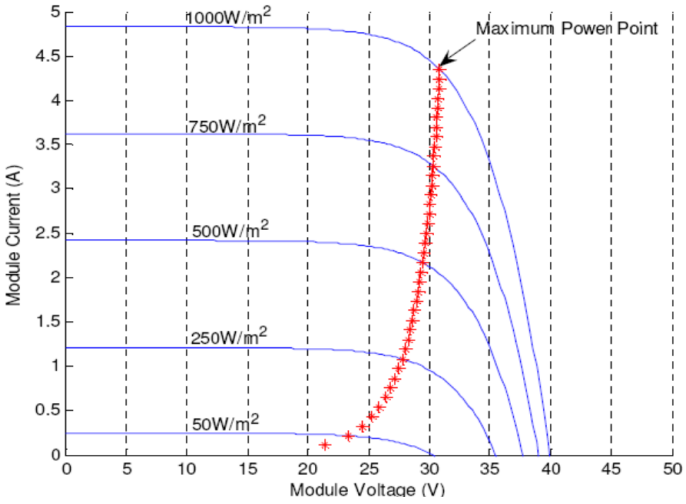

Figure 2. *The V-I standard curves according to parameters*

JTE
HCMUTE
ISSN: 2615-9740

JOURNAL OF TECHNICAL EDUCATION SCIENCE
Ho Chi Minh City University of Technology and Education
Website: https://jte.edu.vn
Email: jte@hcmute.edu.vn

The *V-I* characteristic depends on the illuminance percentage Kins expressed by the expression:

$$V_g = -0.9I_g + 123{,}69ln\{1{,}0 + 123{,}45(13{,}45K_{ins} - I_g)\} \quad (2)$$

The V-I standard curves according to the illuminance of PV solar cells are shown in Figure 2.

3. Design of the ANFIS and a GA Controller

3.1. GA technology

The ANFIS and GA technologies are employed to find the optimum point for maximum power in any environmental condition. Furthermore, a genetic algorithm is used to optimize data, and optimized values are used to train ANFIS. The following is the procedure for implementing the genetic algorithm [11]. The GA technology is done in the steps below.

- Defining the goal function and identifying the design parameters.
- Defining the initial production population.
- Using the objective function to assess the population.
- If convergence is given, the convergence test is terminated.

The genetic algorithm's goal function is utilized to optimize it. The optimization uses Matlab software to identify the best $Y= (Y_1, Y_2, X_3,..., Y_n)$ to maximize $E_{(X)}$,where the number of design variables is considered 1. $E_{(X)}$ is the array output of the power that should be maximized, and Y is the design variable equivalent to the array current. The administration should be organized depending on the array's current to establish the goal function. Table 1 lists the genetic algorithm settings. When this function is maximized, optimal values for V_{mpp} and MPP will result at any given temperature and irradiation intensity.

Table 1. *GA parameters*

Rank	Parameters	Variable
1	Number of design variable 1	1
2	Population size	20
3	Crossover constant	40%
4	Mutation rate	15%
5	Maximum generations	30

3.2. ANFIS technology

The architecture of the ANFIS with two inputs (x, y) and one output (z) is given in Fig. 3

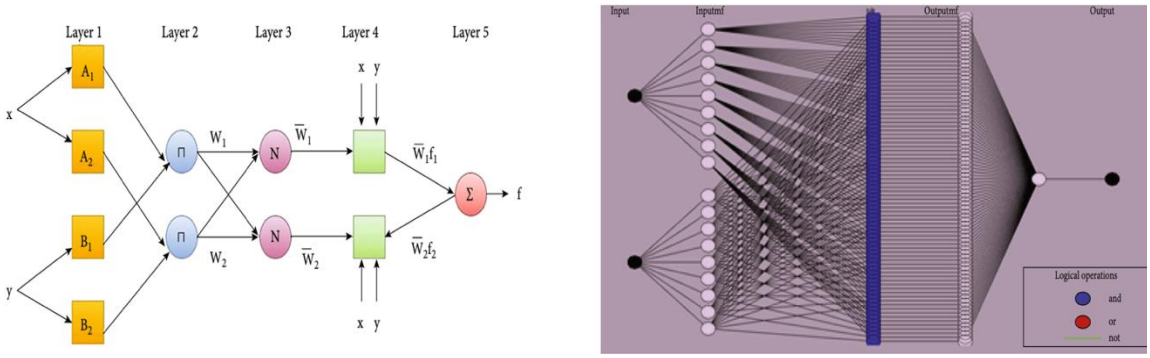

(a) ANFIS achitecture *(b) Type of ANFIS structure*

Figure 3. *ANFIS technology setup for a: ANFIS achitecture and b: Type of ANFIS structure*

In this study, the fuzzy algorithm have 7 fuzzy rules and 7x7 matrix shown in Fig. 4. (a) and (b)

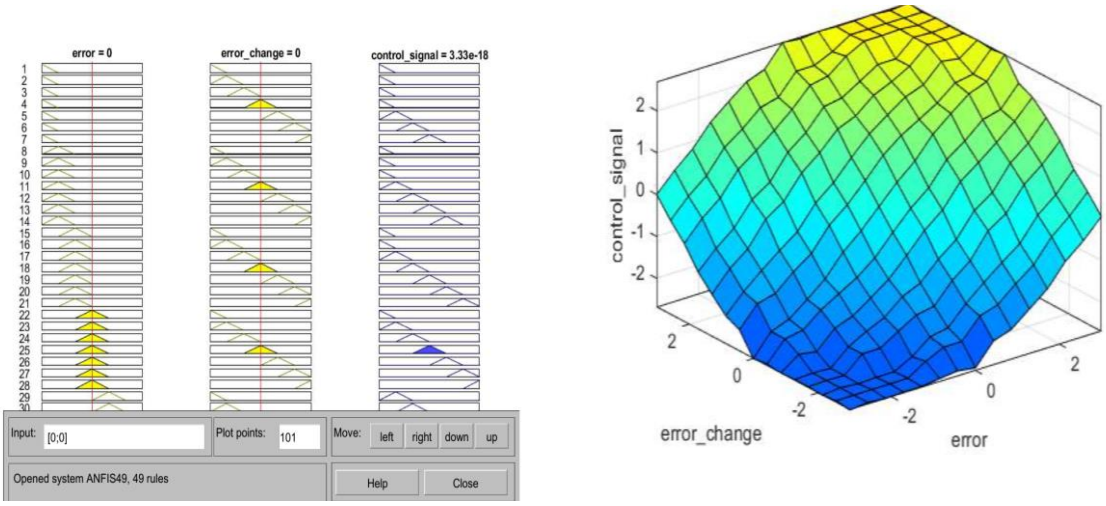

(a) *(b) MATLAB*

Figure 4. *Fuzzy rules setup for a: Image of fuzzy rules in MATLAB and b: Image of fuzzy rule space in MATLAB*

The adaptive ANFIS system combines the functions of neural networks (ANN) and fuzzy logic (FL). An ANN can train a Surgeon fuzzy controller to get the required output signals. The weights of the neural network nodes can also be derived to form a complete rule base. Solar radiation and ambient temperature or PV panel voltage and current can be used as inputs to the PV battery model. An ANN makes it easy to tune function functions and parameter rules. The inference system of the ANFIS controller fits a fuzzy control with the optimization training of nonlinear functions. The unclear authority set for a two-input (m, n)–single-output (z) FIS can be given as:

With rule 1: If *m* is A_1 and *n* is B_1, then $f_1 = p_1x + q_1y + r_1$ (3)

With rule 2: If *m* is A_2 and *n* is B_2, then $f_2 = p_2x + q_2y + r_2$ (4)

The output function is determined using the formula:

$$f = \frac{w_1 f_1 + w_2 f_2}{w_1 + w_2} \quad (5)$$

where: *m* and *n* are inputs; A_1 and B_1 are fuzzy variables; f_i is represent the output in the fuzzy set; q_i and q_i are the parameters selected during the training of ANFIS.

The ANFIS algorithm comprises five layers (1 input layer, three hidden layers, and one output layer). The classes are designed as follows:

Layer 1: All neural network nodes are adaptive. At the output of layer 1, there is the i^{th} node in the O_{1i} is depended on the function functions of the corresponding 1^{st} node defined by the formula:

$$Q_{1,i} = m_{Ei}(x), i = 1.2 \quad (6)$$

$$Q_{1,i} = m_{Fi-2}(y), i = 3 \quad (7)$$

where *x* and *y* are the inputs of node i, and E_i and F_i are the language labels (high or low) associated with the functions of this node $m_{Ei}(x)$ and $m_{Fi-2}(y)$ can use any fuzzy membership function. In this class, the functions used for the inputs x and y are Gaussian.

Layer 2: In layer 2, the neural network nodes are fixed. The layer is related to fuzzy rules, which use the AND neuron operator to fade the input signals. These parameters are labelled π, indicating that the parameters act as a multiplier and are called the neural network layer. The output of layer two is written as follows.

JTE
HCMUTE
ISSN: 2615-9740

JOURNAL OF TECHNICAL EDUCATION SCIENCE
Ho Chi Minh City University of Technology and Education
Website: https://jte.edu.vn
Email: jte@hcmute.edu.vn

$$Q_{2,i} = \omega_i = m_{Ei}(x) * m_{Fi}(y) = 1.2 \quad (8)$$

Layer 3: In layer 3, the fixed neural network nodes are labeled by N. At the output of this layer, O_3 is the sum of neural network nodes activated by previous layers. So the layer three output is shown as follows

$$Q_{3i} = \frac{\omega_i}{\omega_1 + \omega_2}, i = 1,2 \quad (9)$$

Layer 4: Layer 4 outputs are adaptive neural network nodes characteristics and parameters. This fuzzy logic node has parameters like p_i, q_i, r_i. Layer 4 output is shown below the formula:

$$Q_{4i} = \frac{\omega_i}{\omega_1 + \omega_2}(p_i.x + q_i.y + r_i.), i = 1,2 \quad (10)$$

Layer 5: In layer 5, there is only one fixed node, and the output is calculated as the sum of all incoming signals. The output function of the 5th layer is shown in the equation.

$$Q_{5i} = \frac{\widehat{M_i}}{\widehat{M_l}} \frac{\omega_i f_i}{\omega_i} \quad (11)$$

4. Boost converter

4.1. The average model of the boost converter

The diagram boost converter in Fig. 5 switching network includes valve MOSFET and diode. Because the input current to port one $i_1(t)$ is the current through the inductor. The current can be considered an independent variable. The output voltage on the capacitor $v_2(t)$ is the voltage on the load that changes only when the load changes, so also considered is the independent variable. Therefore, voltage $v_1(t)$ and $i_2(t)$ are dependent variables.

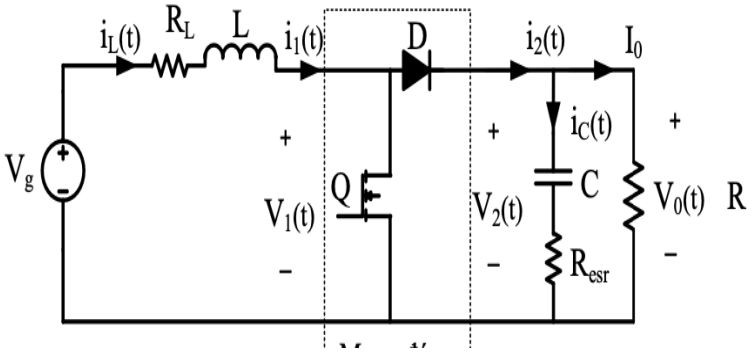

Figure 5. *The switching circuit in the diagram boost converter*

Average voltage $v_1(t)$ and current $i_2(t)$ over a period T_s assuming $v_2(t)$ and $i_1(t)$ pulses are negligible or vary almost linearly are written by Eq.(6) &(7).

$$(V_1(t))_{T_s} = (1 - d(t))(V_2(t))_{T_s} = d'(t)(V_2(t))_{T_s} \quad (12)$$

$$(i_1(t))_{T_s} = (1 - d(t))(i_1(t))_{T_s} = d'(t)(i_2(t))_{T_s} \quad (13)$$

The average model of the boost converter is shown in Fig.6.

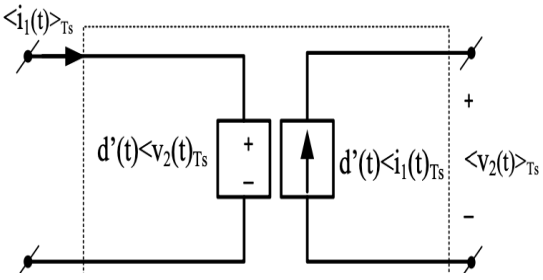

Figure 6. *Average model for boost converter*

Proceed to linearize the model on Fig. 5 by introducing small fluctuations:

$$\begin{pmatrix} V_g(t) = V_g + \widehat{V_g}(t) \\ i_L(t) = I_L + \widehat{i_L(t)} \\ V_1(t) = V_1 + \widehat{V_1(t)} \\ i_2(t) = I_2 + \widehat{i_2}(t) \\ V_2(t) = V_2 + \widehat{V_2}(t) \\ d = D' + \widehat{d(t)} \\ d' = 1 - d = D' + \widehat{d(t)} \end{pmatrix} \quad (14)$$

The dependent voltage source at input port 1 becomes:

$$\langle V_1(t)\rangle = d'(t)\langle V_2(t)\rangle = \left(D' - \hat{d}(t)\right)\left(V_2 + \widehat{V_2}(t)\right) \approx D'\left(V_2 + \widehat{V_2}(t)\right) - V_2\hat{d}(t) \quad (15)$$

First term $D'\left(V_2 + \widehat{V_2}(t)\right)$ shows the dependence on the output voltage $V_2 + \widehat{V_2}(t)$ in proportion D', described by the dependent voltage source. Rank $V_2\hat{d}(t)$ is the source controlled by the modulation factor $\hat{d}(t)$ should become an independent voltage source connected in series in the circuit.

The dependent current is shown:

$$\langle i_2(t)\rangle = d'(t)\langle i_1(t)\rangle = \left(D' - \hat{d}(t)\right)\left(I_1 + \widehat{I_1}(t)\right) \approx D'\left(I_1 + \widehat{i_1}(t)\right) - I_1\hat{d}(t) \quad (16)$$

Rank $D'\left(I_1 + \widehat{i_1}(t)\right)$express dependence on $\left(I_1 + \widehat{I_1}(t)\right)$ in proportion D′ should be described by the dependent current source. Rank $I_1\hat{d}(t)$is the current source controlled by the factor $\hat{d}(t)$ become an independent current source in parallel with the circuit. From there, the average model of the switching network for the boost circuit.

From the above analysis, the average model for the boost converter is shown Fig.7:

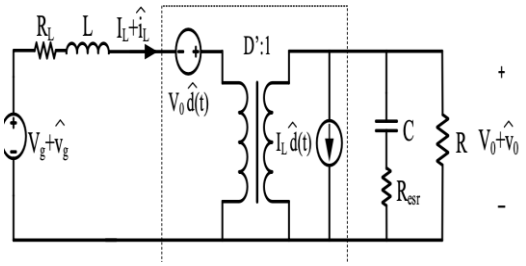

Figure 7. *Average model for Boost circuit*

Considering the small signal model as shown in Fig.6. This model is necessary to determine the critical transfer functions for the design of the current controller:

$$\begin{cases} G_{VD} = \dfrac{\widehat{v_0}}{\hat{d}}\Big|\ \widehat{v_g} = 0 \\ G_{id} = \dfrac{\widehat{I_L}}{\hat{d}}\Big|\ \widehat{v_g} = 0 \end{cases} \quad (17)$$

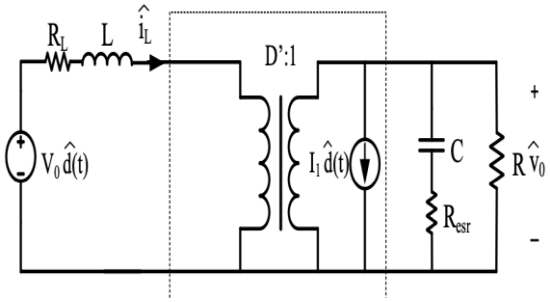

Figure 8. *Small signal average model for boost circuit when* $\widehat{v_g} = 0$

JTE
HCMUTE
ISSN: 2615-9740

JOURNAL OF TECHNICAL EDUCATION SCIENCE
Ho Chi Minh City University of Technology and Education
Website: https://jte.edu.vn
Email: jte@hcmute.edu.vn

To find these transfer functions, we remove the influence of the source $\widehat{v_g} = 0$ in the model Fig. 8 & 9 to obtain a simple model.

Next, convert to the transformer's primary, Laplace the circuit, and then, based on the circuit calculation, derive the desired transfer function G_{vd} and G_{id}.

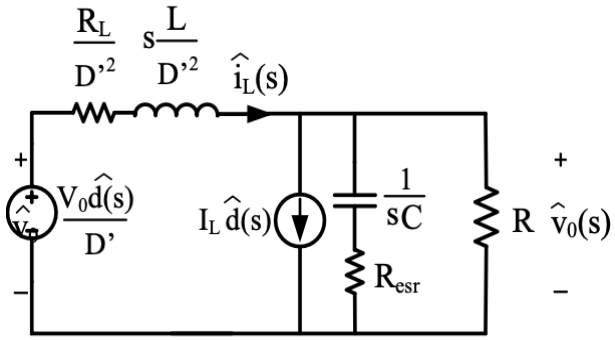

Figure 9. *Laplace of the converter circuit*

The voltage balance in the circuit shown in Eq. (18) is obtained:

$$G_{vd}(s) = \frac{\widehat{V_0}(s)}{\hat{d}(s)} = \frac{V_0}{D'} \frac{\left(1 - \frac{R_L + sL}{RD'^2}\right)(1 + sR_{esr}C)}{s^2 \frac{LC(R + R_{esr})}{RD'^2} + s\left(\frac{R_L(R + R_{esr})C + L}{RD'^2} + R_{esr}C\right) + \frac{R_L}{RD'^2} + 1} \quad (18)$$

The current balance in the circuit shown in Eq. (19) is obtained:

$$\hat{\imath}_L(s) = \frac{1}{D'}\left[I_L \hat{d}(s) + \frac{s(R + R_{esr})C + 1}{(1 + sR_{esr}C)R}\hat{v}_0(s)\right] \quad (19)$$

Combined with $\hat{v}_0$t from the transfer function, the transfer function of the current object can be deduced:

$$G_{id}(s) = \frac{\hat{\imath}_L(s)}{\hat{d}(s)} = \frac{V_0}{RD'^2} \frac{(R + 2R_{esr})C + 2}{s\left(\frac{R_L(R + R_{esr})C + L}{RD'^2} + R_{esr}C\right)} + \frac{R_L}{RD'^2} + 1 \quad (20)$$

4.2. Design of current controller

The diagram of the control current is shown in Fig. 10.

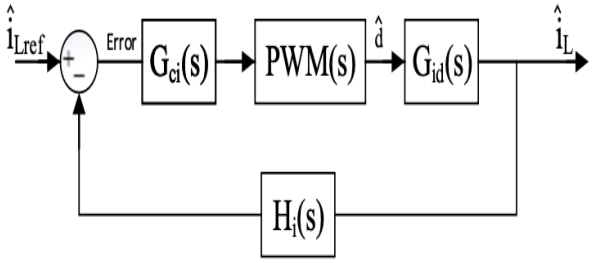

Figure 10. *The diagram of the control current*

The current control loop has fast dynamic characteristics, and the voltage loop has lower dynamic features. As a result, the inductor current can vary very quickly compared to the output voltage.

According to Eq. (20), the transfer function of the current control loop:

$$G_{id}(s) = \frac{0{,}008347s + 48}{1{,}739.10^{-8}.s^2 + 7{,}658.10^{-5}s + 4{,}07} \quad (21)$$

JTE
HCMUTE
ISSN: 2615-9740

JOURNAL OF TECHNICAL EDUCATION SCIENCE
Ho Chi Minh City University of Technology and Education
Website: https://jte.edu.vn
Email: jte@hcmute.edu.vn

5. Matlab results

The MATLAB simulations of structure GA-ANFIS-MPPT controller using a boost converter is built as shown in Fig. 10. MATLAB has a module string, one parallel string, and a 250W PV panel. The input temperatures are 25^0C, the irradiances range from 50 W/m^2 to 1000 W/m2.

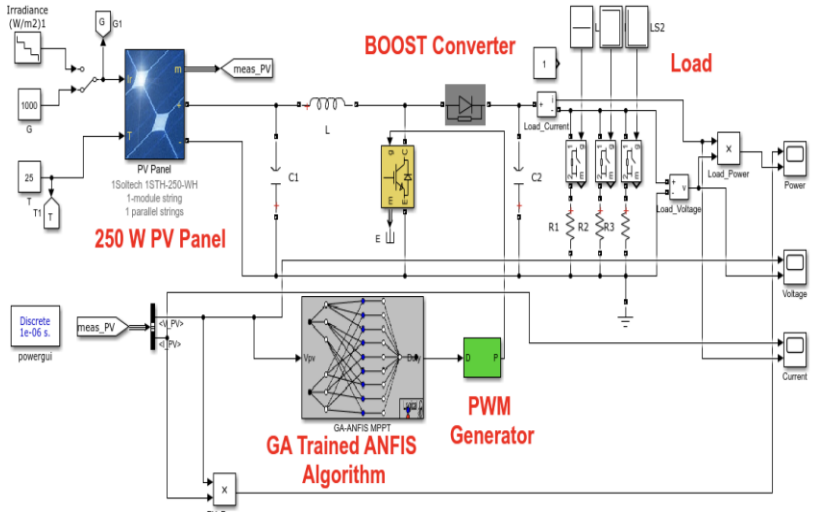

Figure 11. *The MATLAB simulations GA-ANFIS-MPPT controller using a boost converter*

To precisely analyse the performance of the GA-ANFIS technique, the simulation is conducted for different PV and load currents at a constant temperature (25^0C) with a fixed insolation flow step, as shown in Fig.12 (a). Fig. 12(a) shows the load current variation from 3 to 0.5A, meanwhile, the PV current variation from 8 to 1.9 A. The PV and load voltages is indicated in Fig.12 (b). Fig. 12(b) shows the variation in the load voltage from 40 to 100 V. Meanwhile, the PV voltage is constant with 32V at 0,08s. The PV and load power is indicated in Fig.13. Fig.13 shows the variation in the load and PV powers from 250 to 50 V.

Based on MATLAB/SIMULINK results, the GA-ANFIS method shows a smoother power, less oscillating, and a better stale operating point. Regarding power stabilization, the PV power controlled by ANFIS-GA is durable.

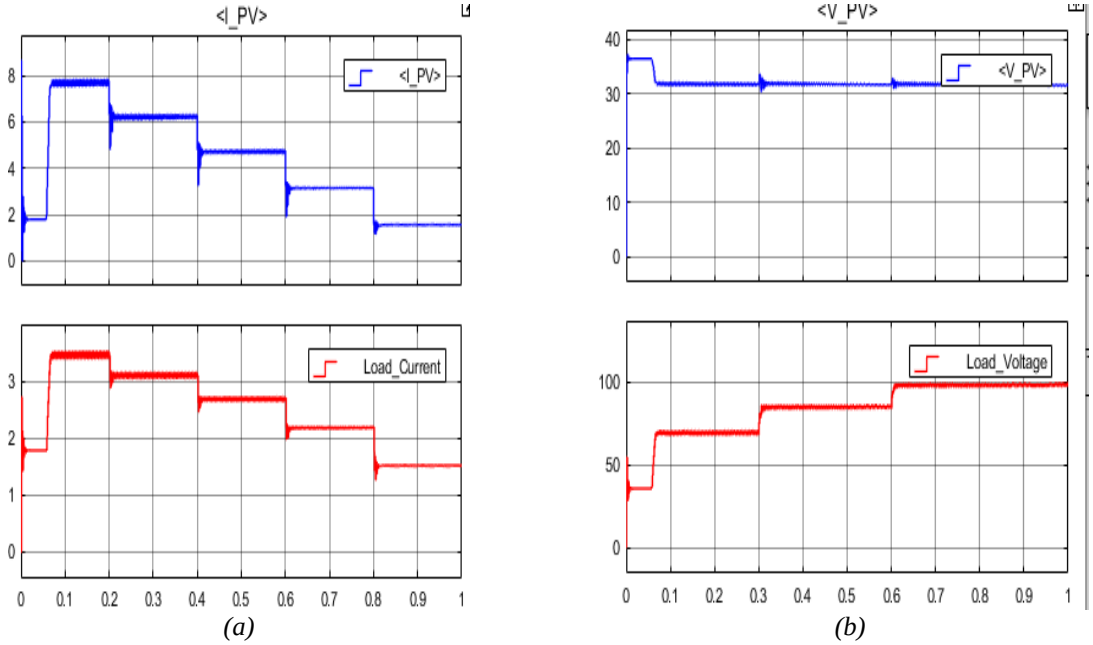

Figure 12. *Simulated results for PV for a: The PV and load currents; b: The PV and load voltages*

JTE
HCMUTE
ISSN: 2615-9740

JOURNAL OF TECHNICAL EDUCATION SCIENCE
Ho Chi Minh City University of Technology and Education
Website: https://jte.edu.vn
Email: jte@hcmute.edu.vn

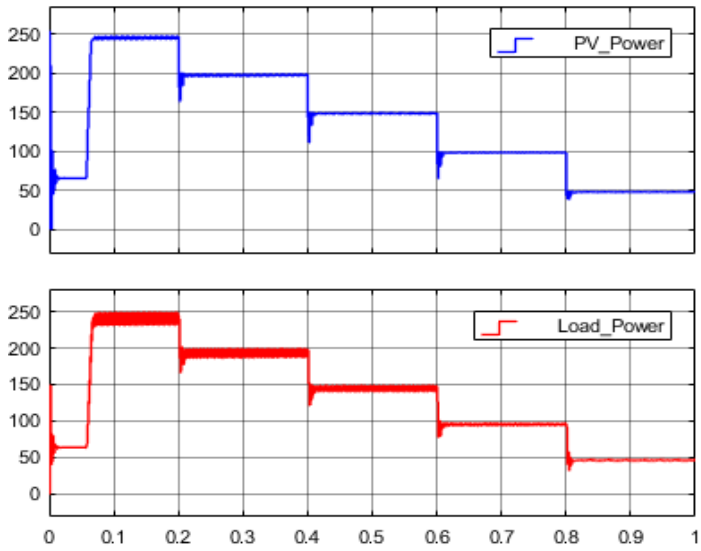

Figure 13. *Simulated results for PV and load power*

Fig.14 (a) shows that the ANFIS test output was compared with the target values. Fig.14 (b) is shown the data test error. The network is trained for 200 epochs. After the training process, output data should be very close to the target outputs as shown in Fig. 14(c).

Simulated results for Optimized values were used for training the GA-ANFIS is shown Fig.14. For various conditions, the proposed method was verified, and it found that the error percentage of V_{mpp} was between -0.05% to 0.04%. Incrementing the number of training data could be diminished the error of ANFIS.

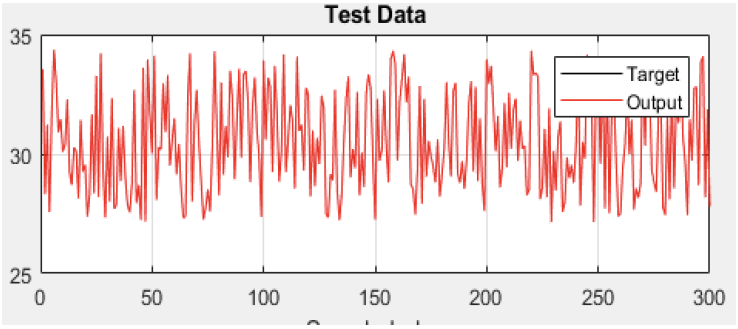

(a)

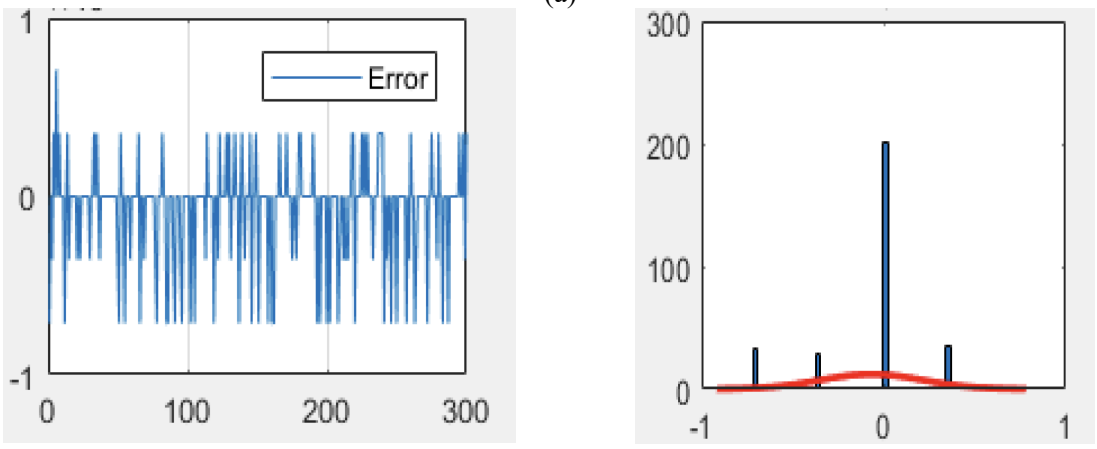

(b) (c)

Figure 14. *Simulated results for optimized values were used for training the GA-ANFIS*

6. Conclusions

This work included designing, modelling, and evaluating the proposed GA-ANFIS-based MPPT controller. The solar module's real-time MPP was constantly tracked to determine the maximum power output a PV module can generate given a particular set of sun irradiation and temperature conditions. The proposed MPPT controller's components and subsystems were modelled and simulated in the MATLAB/SIMULINK environment. The simulation results show that the proposed GA-ANFIS-based MPPT can reliably and effectively monitor the maximum power point of PV modules under various meteorological conditions. The control signal for the boost converter was generated using the proposed ANFIS power controller, yielding satisfactory MPPT results. The methodology's usefulness will be shown in the future by applying the study findings to real devices and comparing them to other control approaches.

Acknowledgments

This project study was supported by all researchers and funding from the University of Transport and Communications.

REFERENCES

[1] P. A. Owusu and S. A. Sarkodie, "A Review of Renewable Energy Sources, Sustainability Issues and Climate Change Mitigation," *Cogent. Eng*., vol. 3, no. 1, pp. 1–14, 2016.
[2] C. Wan, J. Zhao, Y. Song, Z. Xu, J. Lin, and Z. Hu, "Photovoltaic and solar power forecasting for smart grid energy management," *CSEE J. Power Energy Syst*., vol. 1, no. 4, pp. 58-46, Dec. 2015.
[3] J. Antonanzas *et al*., "Review of photovoltaic power forecasting," *Sol. Energy*, vol. 136, pp. 78-111, Oct. 2016.
[4] I. I. R. E. Agency, "Renewables Account for Almost Three Quarters of New Capacity in 2019," *IRENA*. Accessed 2020. [Online]. Available: https://www.irena.org/newsroom/pressreleases/2020/Apr/Renewables-Account-for-Almost-Three-Quarters-of-New-Capacityin-2019.
[5] M. H. Ahmadi *et al*., "Solar Power Technology for Electricity Generation: A Critical Review," *Energy Sci. Eng*., vol. 6, no. 5, pp. 340–361, 2018.
[6] M. Malinowski, J. Leon, and H. Abu-Rub, "Solar Photovoltaic and Thermal Energy Systems: Current Technology and Future Trends," *Proc. IEEE*, vol. 105, no. 11, pp. 1–15, 2017.
[7] J. Hossain and A. Mahmud, *Renewable Energy Integration: Challenges and Solutions*, New York, USA: Springer Science & Business Media, 2014.
[8] M. R. Hamzescu and S. Oprea, *Practical Guide to Implementing Solar Panel MPPT Algorithms*, Microchip Technology Inc., Arizona, USA, 2013.
[9] S. Cherukuri, "A Novel Global MPP Tracking of Photovoltaic System based on Whale Optimization Algorithm," *Int. J. Renew. Energy Dev*., vol. 5, p. 225, 2016.
[10] A. A. A. Mohamed, A. L. Haridy, and A. Hemeida, "The Whale Optimization Algorithm based controller for PMSG wind energy generation system," in *Proceedings of the 2019 International Conference on Innovative Trends in Computer Engineering (ITCE)*, Aswan, Egypt, 2–4 Feb. 2019, pp. 438–443.
[11] K. S. Tey *et al*., "Improved Differential Evolution-Based MPPT Algorithm Using SEPIC for PV Systems Under Partial Shading Conditions and Load Variation," *IEEE Trans. Ind. Inform*., vol. 14, pp. 4322–4333, 2018.
[12] K. Guo *et al*., "An Improved Gray Wolf Optimizer MPPT Algorithm for PV System with BFBIC Converter Under Partial Shading," *IEEE Access*, vol. 8, pp. 103476–103490, 2020.
[13] B. Parida, S. Iniyan, and R. Goic, "A review of solar photovoltaic technologies," *Renew. Sustain. Energy Rev*., vol. 15, pp. 1625–1636, 2011.
[14] M. Veerachary, T. Senjyu, and K. Uezato, "Neural-networkbased maximum-power-point tracking of coupled inductor interleaved-boost-converter-supplied PV system using fuzzy controller," *IEEE Trans. Ind. Electron*., vol. 50, no. 4, pp. 749–758, 2003.
[15] A. K. Rai *et al*., "Simulation model of ANN based maximum power point tracking controller for solar PV system," *Solar Energy Materials and Solar Cells*, vol. 95, no. 2, pp. 773–778, 2011.
[16] A. Rezvani *et al*., "Investigation of ANN-GA techniques for photovoltaic system in the grid connected mode," *Indian Journal of Science and Technology*, vol. 8, no. 1, pp. 87–95, 2015.
[17] J. Yang and V. Honavar, "Feature subset selection using a genetic algorithm," *IEEE Intelligent Systems*, vol. 13, no. 2, pp. 44–49, 1998.

Vo Thanh Ha received a bachelor's degree in Control and Automation Engineering from the Thai Nguyen University of Technology, Vietnam, in 2002. She received a master's degree from Hanoi University of Science and Technology, Vietnam 2004. She received a Ph.D. in Control and Automation Engineering from Hanoi University of Science and Technology, Viet Nam, in 2020. She has worked at the University of Transport and Communications as a lecturer since 2005. Her current areas of research are electrical drive and electric vehicles. She can be contacted at email: vothanhha.ktd@utc.edu.vn.